Proceedings of the
Annual Stability Conference
Structural Stability Research Council
Louisville, Kentucky, April 1-4, 2025

Stability and response of lacing systems in laced built-up truss bridge columns

Oudom Chhoeng[1], Morane Chloé Mefande Wack[2], Robert Tremblay[3], Nicolas Boissonnade[4]

Abstract

Laced built-up members were often used in old truss steel bridge members. These members often comprise plates, channels, and angle sections connected by various lacing systems such as lacing bars or angles. According to current design practices, the main components of built-up sections are designed to reach failure load before the transverse members. The inclusion of lacing systems aims to ensure that each main component behaves together as a member to achieve the highest capacity. AISC recommends that lacing members shall be able to resist shear force equal to 2% of the available compressive strength of the built-up member. The Standards specify dimensional requirements for both built-up and lacing members, while AASHTO provisions adopted similar suggestion to AISC yet impose limits on the slenderness of built-up members. However, existing bridge members may not always meet these design requirements and several questions regarding the influence of lacing stability and lacing arrangement on the shear force and compressive strength of built-up members remain. This paper studies a wide range of non-linear numerical models of laced built-up members consisting of pairs of hot-rolled C-shape sections interconnected with double (X) and single (diagonal) flat lacing bars. The developed models are validated against existing test data. The study further discusses the impact of lacing arrangement and the overall stability of lacing members under shear force. The numerical results are then used to evaluate a proposed design shear force equation for the lacing system, showing it provides more accurate and consistent predictions than current design recommendations.

1. Introduction

Built-up members are commonly found in older truss steel bridge structures. These members, as depicted in Figure 1, typically consist of plates, channels, and angle sections, linked by transverse elements like batten plates, lacing bars, or perforated plates. In laced members with angles, lacing bars may be applied on all four sides, or the angles can be paired with continuous web plates to create two C-sections. To calculate the capacity of steel built-up members, the lacing system must be capable of resisting the internal forces in the connecting elements before the member fails. Figure 2a illustrates a typical laced built-up member under compression. In such cases, the lacing system's strength is crucial for the member's stability. This is especially important for built-up members with initial global deflections (Figure 2b), where the lacing members must resist internal

[1] PhD candidate, Polytechnique Montréal, <oudom.chhoeng@polymtl.ca>
[2] PhD candidate, Polytechnique Montréal, <morane-chloe.mefande-wack@polymtl.ca>
[3] Professor, Polytechnique Montréal, <robert.tremblay@polymtl.ca>
[4] Professor, Université Laval, <nicolas.boissonnade@gci.ulaval.ca>

forces. These forces, such as bending moments and shear forces, are calculated based on the deformed shape (second-order analysis), as shown in Figure 2c. For design, these forces are distributed to the diagonal lacing members, which may experience either compression or tension, as depicted in Figure 2d.

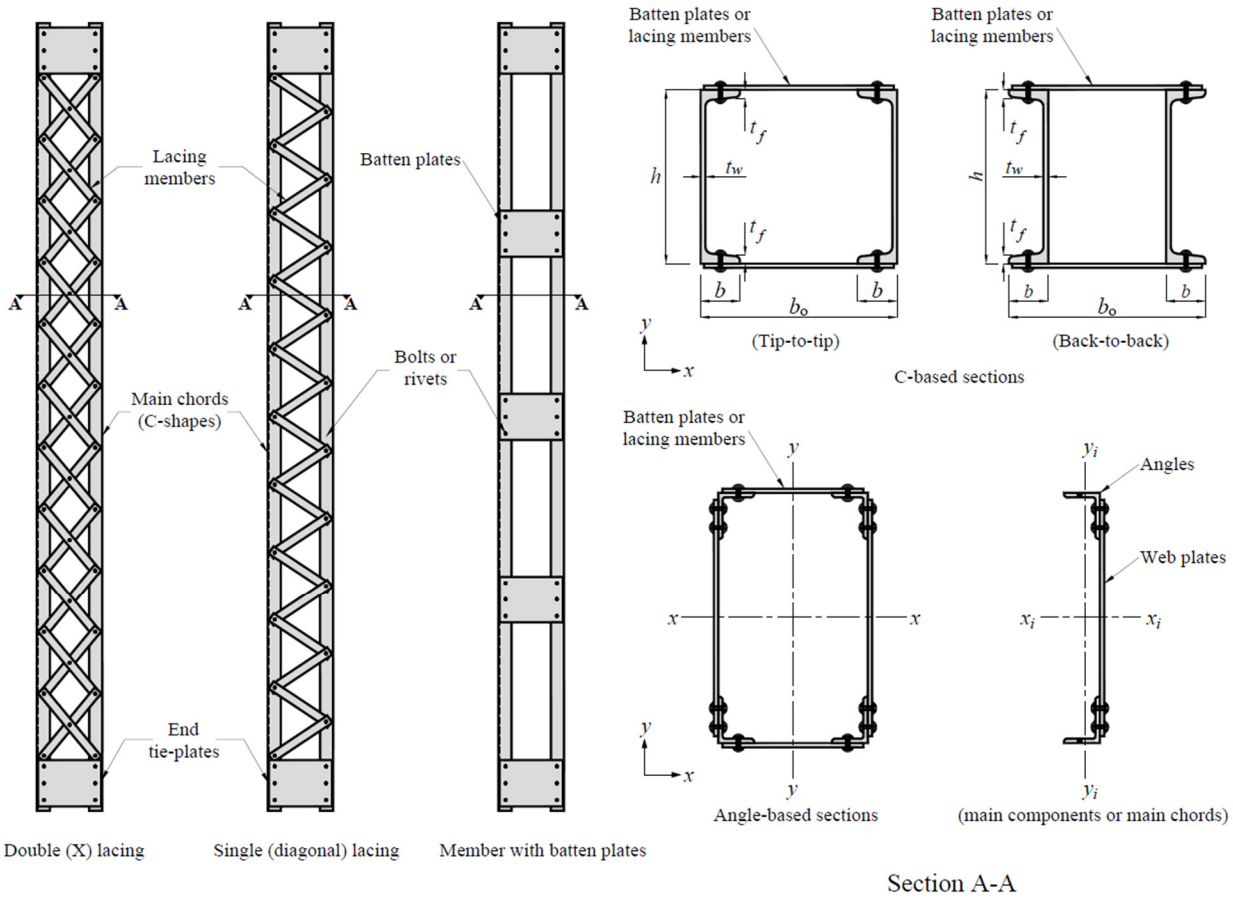

Figure 1: Notations and typical built-up members are commonly used in steel truss bridges.

The current design approach for built-up compressive members ensures that the main components fail before the connecting elements. The connecting elements, such as lacing bars, are included to make the main components function as a single unit for higher capacity and to resist shear forces from bending and external loads. According to EC 3, shear force is calculated based on the maximum second-order moment at the midpoint of a built-up member, which is caused by an initial deflection of the entire member. This second-order moment is computed for built-up compression members with hinged ends, considering an initial bow imperfection e_0 and the first-order bending moment at the midsection M^I, where e_0 is equal to $L / 500$. The elastic shear deformation of the lacing system is assumed to be continuous and is determined from the column's shear stiffness S_v, which varies based on the lacing arrangement. For a single lacing system with two planes of lacings, S_v is expressed as follows:

$$S_v = \frac{EA_d ch_0^2}{d^3} \tag{1}$$

For double lacing system with two planes of lacings, S_v is given by:

$$S_v = \frac{2EA_d ch_0^2}{d^3} \tag{2}$$

Here, A_d is the cross-sectional area of lacing members, h_0 is the distance between the centroids of the chords, and c and d represent the distance between connectors and the length of diagonal, respectively (see Figure 2). In contrast to the EC 3 approach, the AISC Standard provides a simplified equation for calculating the design shear force in built-up members. For single and double lacing systems, the minimum shear force is set at 2% of the available compressive resistance N_u of the built-up member, as long as the slenderness ratio does not exceed 140 for single lacing and 200 for double lacing. This criterion applies if the angle of the lacing to the axis of the built-up member is at least 60 degrees for single lacing and 45 degrees for double lacing. However, the AASHTO provisions do not specify a recommended design shear force for laced built-up members, apart from an additional restriction from the AISC Standard. This restriction limits the slenderness ratio of the built-up member to 120 for primary truss members and 140 for secondary truss members.

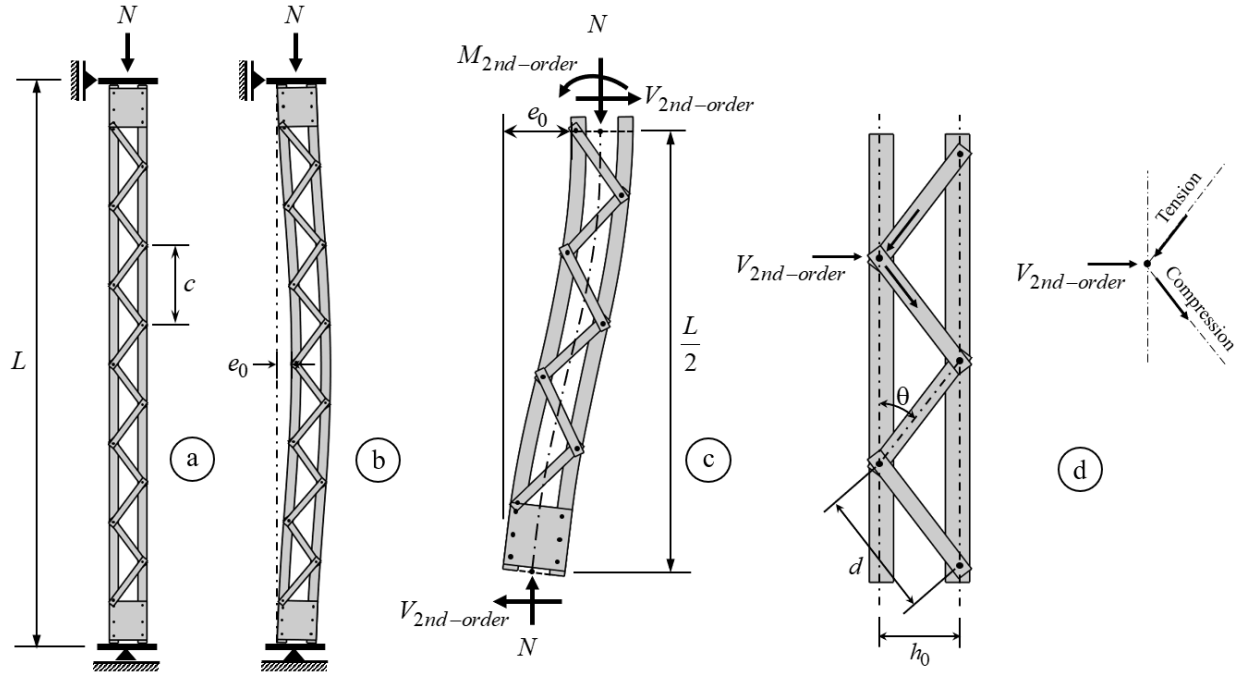

Figure 2: Second-order effects in laced built-up columns.

The American Standards set dimensional limits for the lacing system, but the equations for determining the design shear force are limited because they depend on the specific dimensions of the lacing member. Many older truss bridge members, particularly those built in the 1950s, may not meet the slenderness limits defined by the current standards. Additionally, the equations from both standards do not consider shear deformations caused by flexural buckling instability in the lacing member, meaning the slenderness effect of the lacing member should be taken into account. Therefore, the design rules need to be updated, especially for members that do not meet the dimensional requirements set by the code. Specifically, improvements should (i) address potential

buckling in the lacing members and (ii) consider the impact of different lacing arrangements on second-order shear forces in built-up members. The formulas for predicting shear forces V_u in built-up members, as suggested by both standards, are summarized in Table 1.

Table 1: Design 2nd order shear force provided by current design standards.

Codes	Design shear force in built-up members
EC 3	$V_u = \frac{\pi M_u}{L}$ Where $M_u = \frac{N \cdot e_0 + M^I}{1 - N/N_{cr} - N/S_v}$
AISC & AASHTO	$V_u = 0.02 N_u$

2. Numerical investigations

2.1 Basic features of numerical models

The finite element models of the laced built-up members were created using the non-linear Finite Element (FE) software ABAQUS. The built-up sections are widely spaced components, consisting of two longitudinal columns (main chords) arranged either tip-to-tip ([ ]) or back-to-back (] [), referred to as the main chords. These main chords are connected by flat lacing bars, which are arranged in either X-configurations (double lacing) or diagonal-configurations (single lacing) at intermediate spans and are reinforced with tie-plates at both ends. The four-node shell element (S4R) was selected to model the main chords, lacing bars, and tie-plates, as it has been shown to provide excellent accuracy in previous studies on mono-symmetric and plate sections. A mesh size of 1/20th of the web dimension of the main chords was chosen, as it provided a good balance between computational efficiency and numerical accuracy and was used for further investigations.

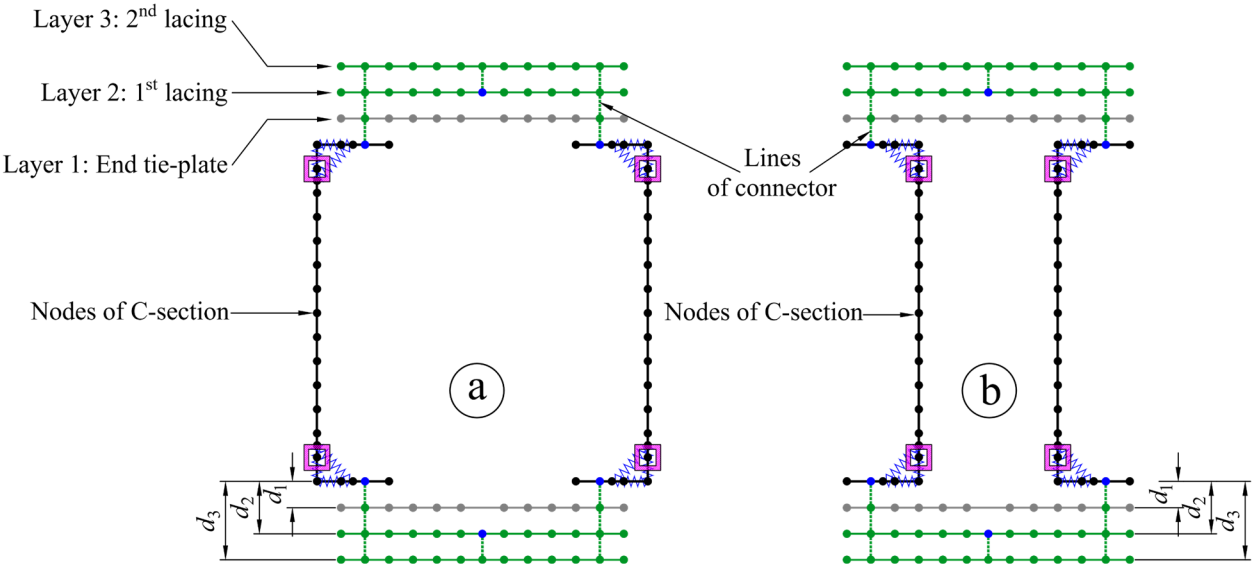

Figure 3: Cross-sectional modeling – (a) Tip-to-tip section – (b) Back-to-back section.

Figure 3 shows the numerical model considered for laced built-up members. All tie-plates and lacing members are connected to the flange of the main component through a line of connectors. The cross-sectional model of the main C components is composed of three shell plates with constant thickness, leading to problems at the joint areas by forming the missing fillet areas and

overlapping areas (see Figure 4a). For hot-rolled sections, the absence of fillet zones in the FE model decreases the actual second moment of area and torsional stiffness of the cross-section (especially St Venant's torsional stiffness) (Li and Boissonnade 2022). As depicted in Figure 4b, extra square hollow beam sections were added to the cross-sectional model at the center gravity of radius zones. Since the missing area is equal to the intersection of the flange plate and web plate, this improvement enables the model to more accurately capture the section area by including the fillet area, thereby providing additional torsional. Furthermore, additional spring elements with strong stiffness were added to the fillet zones of the section to prevent local buckling in these areas, ensuring that local buckling occurs outside the fillet areas of the flanges and web plates.

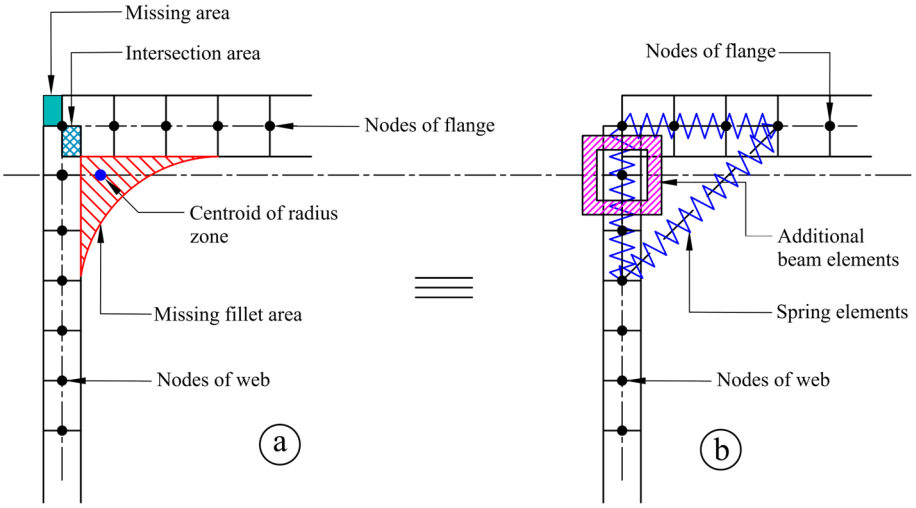

Figure 4: Modeling the joint between the web and flange of a main component.

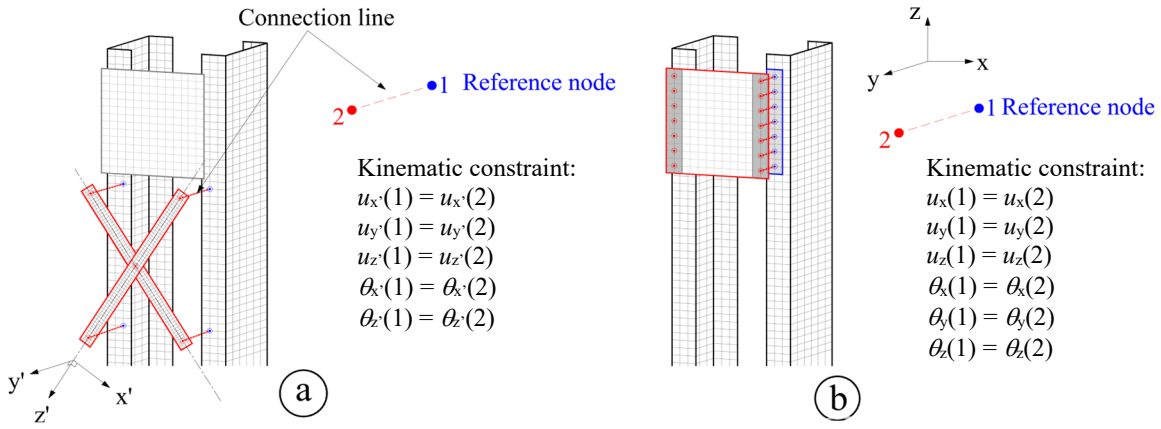

Figure 5: Connection modeling – (a) Connection between tie-plates to main chord – (b) Connection between lacing members to main chord.

The "rivet connector" is assumed to behave in such a way that rotation is free, meaning the lacing bar is free to rotate in the plane of the lacing system. Figure 5a shows the connection line between two corresponding nodes of the lacing member and the chord, representing the rivet connection. A kinematic constraint is assigned through this connection line, allowing both nodes, i.e., reference node (node 1) and coupling node (node 2), to share the same translational degrees of freedom in the x', y', and z' directions, as well as the same rotational degrees of freedom around the x' and z' axes. The rotational degree of freedom around the longitudinal axis of the rivet, i.e., the y' axis, is

not constrained, allowing both nodes to rotate freely around this axis. All degrees of freedom of the coupling node are defined with respect to the reference node located on the chord. Finally, the end tie-plates are connected to the chord member by using the tie constraint, representing either a rivet or bolted connection. As depicted in Figure 5b, a similar approach has been followed and kinematic constraints have been defined to ensure that each node in the connected area shares the same displacement and rotation.

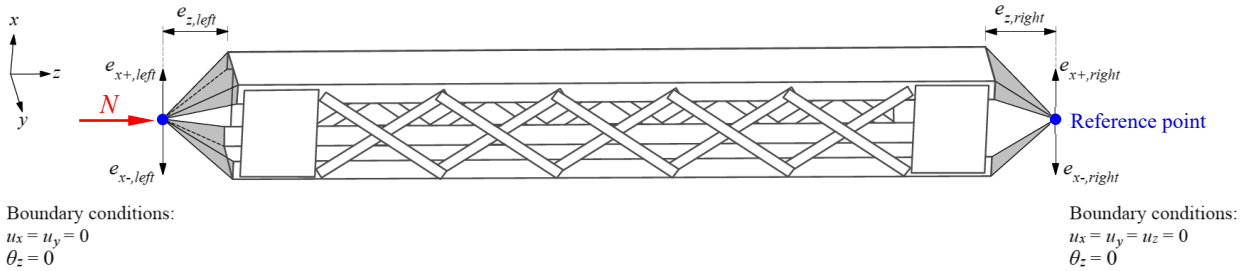

Figure 6: Boundary conditions of built-up members in the numerical models.

The boundary conditions of the built-up column were defined as pinned-pinned, as shown in Figure 6. All nodes at each end of the member were constrained to have the same displacement as the reference point, which is located at the center of gravity of the cross-section. Torsional rotation and translational displacement along the x and y directions were restrained at both ends, with constraints $u_x = u_y = \theta_z = 0$. The load was applied to the model through the reference point at one end in the axial direction (z direction), while the axial displacement at the opposite end was restricted ($u_z = 0$). To accurately represent the actual support position and loading conditions when the FE models are used to replicate experimental setups, the position of the reference point could be adjusted translationally and longitudinally by specific distances e_x and e_z, respectively. The material model employed was a quad-linear stress-strain relationship, characterized by an elastic linear portion, a yield plateau, and a two-stage non-linear strain hardening. This relationship was calibrated into true stress and logarithmic plastic strain as required within the ABAQUS environment.

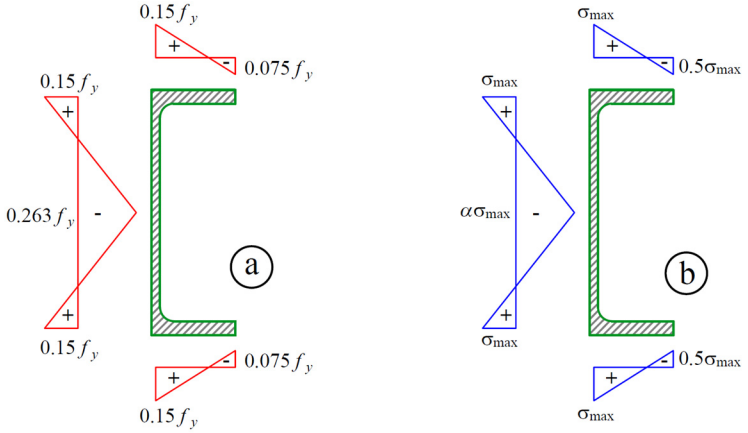

Figure 7: Residual stresses proposed in the literature – (a) Reduced residual stresses for C sections in (Lindner and Glitsch 2004) – (b) Proposed residual stresses for C sections in (Beyer et al. 2018).

In the modeling of residual stress for C-sections, an intriguing challenge arises due to the lack of experimental data for hot-rolled channel sections. Given this constraint, most researchers have resorted to adapting existing data from related profiles, such as hot-rolled I shape sections. This

approach was notably employed by Lindner and Glitsch (Lindner and Glitsch 2004), who proposed a methodology to extract residual stress patterns from I shape sections and subsequently adjusted them to suit channel sections (see Figure 7a). This residual stresses pattern was later further used by Beyer et al. (Beyer et al. 2018), who proposed residual stresses distribution patterns in finite element models for UPE sections subjected to major-axis bending. The authors suggested to take $\sigma_{max} = 0.15 f_y$ and $\alpha = 1 + b t_f / (h t_w)$.

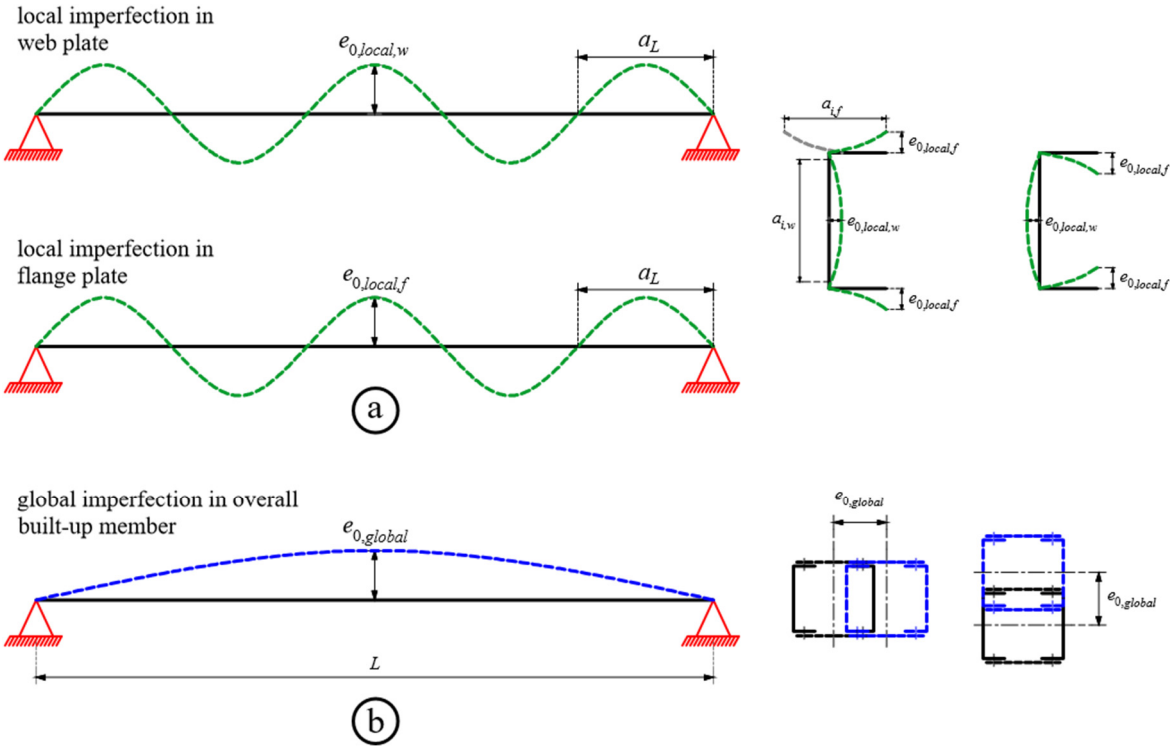

Figure 8: Definition of – (a) Local geometrical imperfections – (b) Global geometrical imperfections.

The geometrical imperfections are introduced both locally and globally by adjusting the coordinates of nodes using sinusoidal functions (see Figure 8). Local imperfections, affecting the web and flange plates, are characterized by plate buckling lengths $a_{i,w}$ and $a_{i,f}$, respectively. Specifically, $a_{i,w} = h - 2(t_f + r)$, while $a_{i,f} = 2(b - t_w - r)$. For local imperfections, the amplitude $e_{0,local,i}$ is taken as a_i / 200, as suggested by Eurocode 3 Part 1.5 and by Gérard et al. (Gérard et al. 2021) for I sections. These amplitude values are applied independently to each plate, where a_i corresponds to each "plate buckling length". The half-wave length a_L, defined as the average of the web and flange buckling lengths, $a_L = (a_{i,w} + a_{i,f}) / 2$, is chosen here since it has been reported by Gérard et al. 2019 (Gérard et al. 2019) to provide reasonable and appropriate resistance predictions. As depicted in Figure 8a, an odd number of half-waves is used to maintain the weakest cross-section located at mid-span along the member's length. The global imperfection, denoted as $e_{0,global}$ is introduced along the minor-axis.

2.2 Validation of numerical models

The FE models were validated against 23 test results reported in (Astaneh-Asl et al. 1998), (Kleiser and Uang 1999), (Lee and Bruneau 2008), (Bonab, et al. 2013), and (Kalochairetis et al. 2014). The tests cover 10 laced built-up members where the main components are composed of four

angles connected in pairs with continuous web plates to form two C sections (4L+2P), as well as 13 laced built-up members where the chord members consist in two channel sections (2C). The lacing configuration, test loading, loading positions, and the results of the validation study, i.e., ultimate load of test ($N_{u,test}$) and FE model ($N_{u,FE}$) and the load ratio $N_{u,FE}$ / $N_{u,test}$, are presented in Table 2 for specimens loaded under cyclic conditions and Table 3 for specimens loaded under static conditions. In Table 2, the three tests reported by Astaneh-Asl et al. (Astaneh-Asl et al. 1998) and (Astaneh-Asl et al. 1998) and Kleiser and Uang 1999 (Kleiser and Uang 1999) utilized specimens fabricated to represent the back-to-back laced members of San Francisco-Oakland Bay Bridge (SFOBB), with the lacing system riveted to the main components. The as-built specimens were axially loaded with pinned-pinned support at eccentricities (e_x) of 381 *mm*, 127 *mm*, 0 *mm*, respectively. In the test reported by Lee and Bruneau (Lee and Bruneau 2008), the experimental program comprised twelve diagonal bracing members. Since four specimens were closely spaced built-up sections and one specimen (Bx8-60) had setup errors at the beginning of the test, making its results unusable for validating the FE model, only seven specimens (By8-60, By8-120, By16-60, By16-120, Bx8-120, Bx816-60, and Bx16-120) were selected for validation. These specimens consisted of widely spaced built-up sections, fabricated on the basis of data from existing bridges, with lacing members connected to the main components by bolts. All specimens were configured as diagonal bracing members in a rigid frame and subjected to lateral shear forces. According to the experimental setup, all specimens in Table 2 were loaded under displacement control following the ATC-24 cyclic-loading protocol (Case 1). Yet, since this study focuses on the static behavior of the compressive laced built-up members, static loading (Case 2) was also considered.

Table 2: Summary of FE vs. test ultimate load for specimens loaded under cyclic conditions.

Reference	Specimens	Test loadings	Loading positions				Ultimate loads and ratios		
								Case 1	Case 2
			$e_{x,left}$ (*mm*)	$e_{z,left}$ (*mm*)	$e_{x,right}$ (*mm*)	$e_{z,right}$ (*mm*)	$N_{u,test}$ (*kN*)	$N_{u,FE}$ / $N_{u,test}$ (-)	$N_{u,FE}$ / $N_{u,test}$ (-)
(Astaneh-Asl et al. 1998; Kleiser and Uang 1999)	Specimen 1	Cyclic ($N + M_y$)	381	400	0	400	928.79	1.017	0.960
	Specimen 2	Cyclic ($N + M_y$)	127	400	0	400	1633.83	1.012	1.012
	Specimen 3	Cyclic (N)	0	400	0	400	2885.12	0.990	0.954
(Lee and Bruneau 2008)	By8-120	Cyclic (V)	0	0	0	0	295.81	0.952	0.952
	By16-60	Cyclic (V)	0	0	0	0	521.64	0.912	0.911
	By16-120	Cyclic (V)	0	0	0	0	447.00	0.981	0.977
	Bx8-60	Cyclic (V)	0	0	0	0	267.16	1.041	1.047
	Bx8-120	Cyclic (V)	0	0	0	0	213.51	1.113	1.110
	Bx16-60	Cyclic (V)	0	0	0	0	506.87	1.090	1.094
	Bx16-120	Cyclic (V)	0	0	0	0	409.50	1.024	1.024
							Mean	1.013	1.004
							C.o.V.	5.9 %	6.5 %
							Min.	0.912	0.911
							Max.	1.113	1.110

Conversely, the specimens originally loaded under static conditions are presented Table 3. The test programs investigated by Bonab et al. (Bonab et al. 2013) comprise nine specimens, all of which were back-to-back built-up members with a single lacing system. Additionally, the experimental programs reported by Kalochairetis et al. (Kalochairetis et al. 2014) consist in five

groups – Group 1 to Group 5 – of laced built-up sections with double lacing systems. Since the main components of the Group 3 specimen were made of I-sections rather than C-sections, only four groups were selected for validating the numerical model – these members consisted of two C-sections arranged tip-to-tip. In Table 3, all main components of each specimen were interconnected to the lacing system by welding. For lacing with welded connections, an additional rotational constraint, where $\theta_{y'}(1) = \theta_{y'}(2)$, is incorporated into the kinematic constraint shown in Figure 5a. The specimens were set up under simple supports, which the distance between support and the end of member is denoted as e_z, and were loaded under concentric compression load (N). Specimens reported in (Kalochairetis et al. 2014) were subjected to combined compression and bending ($N + M_y$). It is noteworthy that all specimens in Table 3 were constrained to prevent out-of-plane displacement ($u_x = 0$) at the mid-section.

Table 3: Summary of FE vs. test ultimate load for specimens loaded under static conditions.

Reference	Specimens	Test loadings	Loading positions				Ultimate loads and ratios (Case 2)		
			$e_{x,left}$ (mm)	$e_{z,left}$ (mm)	$e_{x,right}$ (mm)	$e_{z,right}$ (mm)	$N_{u,test}$ (kN)	$N_{u,FE}$ (kN)	$N_{u,FE} / N_{u,test}$ (-)
(Bonab et al. 2013)	L140B8(R1)	Static (N)	0	140	0	140	204.76	199.62	0.97
	L140B8(R2)	Static (N)	0	140	0	140	183.86	185.91	1.01
	L140B8(R3)	Static (N)	0	140	0	140	159.09	160.88	1.01
	L140B10(R1)	Static (N)	0	95	0	95	289.05	253.81	0.88
	L170B7(R1)	Static (N)	0	95	0	95	151.95	136.04	0.90
	L170B7(R2)	Static (N)	0	95	0	95	135.19	138.34	0.88
	L170B7(R3)	Static (N)	0	95	0	95	124.32	113.17	0.91
	L170B8(R2)	Static (N)	0	95	0	95	162.40	153.10	0.94
	L170B8(R3)	Static (N)	0	95	0	95	146.29	141.82	0.97
(Kalochairetis et al. 2014)	Group 1	Static ($N + M_y$)	100	162.5	100	162.5	200.00	211.12	1.06
	Group 2	Static ($N + M_y$)	100	162.5	100	162.5	206.00	215.29	1.05
	Group 4	Static ($N + M_y$)	100	162.5	-80	162.5	230.00	246.73	1.07
	Group 5	Static ($N + M_y$)	50	162.5	50	162.5	247.00	250.24	1.01
								Mean	0.985
								C.o.V.	6.3 %
								Min.	0.880
								Max.	1.070

Due to a lack of information on actual measured geometrical imperfections for some specimens and no residual stresses measurements conducted for all test programs, a sensitivity study was initially performed to determine appropriate amplitudes of local and global geometric imperfections, which will later be adopted in numerical parametric studies. Table 4 compares the experimental results with those of the FE numerical predictions for various amplitudes of initial local and global geometric imperfections. The experimental results from Bonab et al. 2013 (Bonab et al. 2013) were not included in Table 4 since the imperfections of those specimens were caused by load repetitions, and the amount of geometric imperfections was determined through a modified Southwell plot (Southwell 1997). The results show that the amplitude combination of $e_{0,local,i} = a_i / 200$ for local imperfection and $e_{0,global} = L / 500$ for global built-up members provides the best mean value ($N_{u,FE} / N_{u,test}$ = 1.006) among all amplitudes, with a C.o.V. of 7.3 %. Therefore, this imperfection combination was adopted for specimens without imperfection measurements and used for further parametric studies in this investigation.

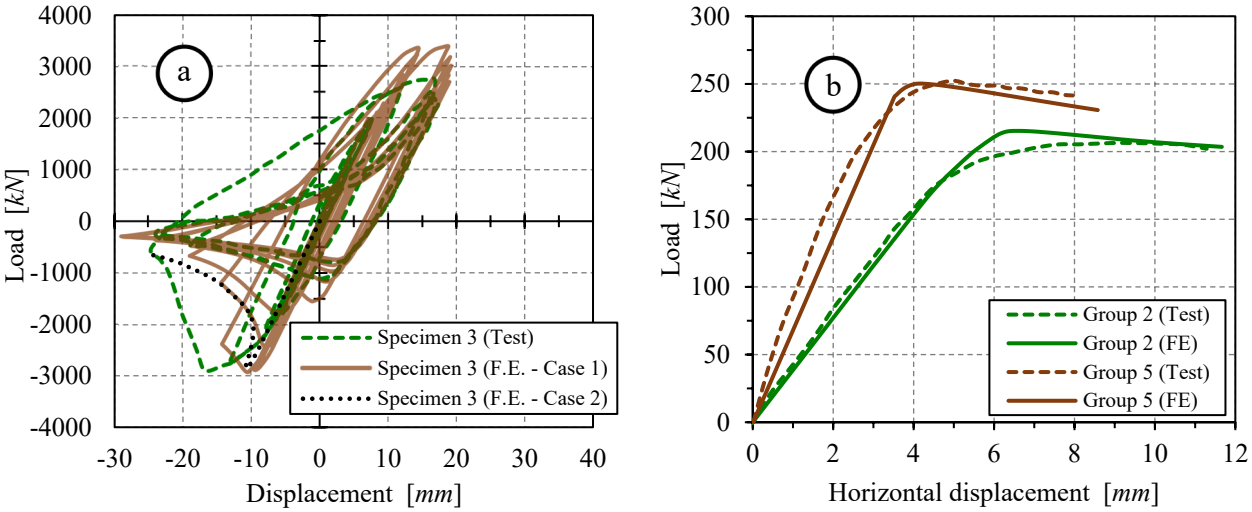

Figure 9: Comparison between test and FE – (a) Hysteretic curve for specimen 3 reported in (Astaneh-Asl et al. 1998) – (b) Load-displacement curves for specimens Group 2 and Group 5 reported in (Kalochairetis et al. 2014).

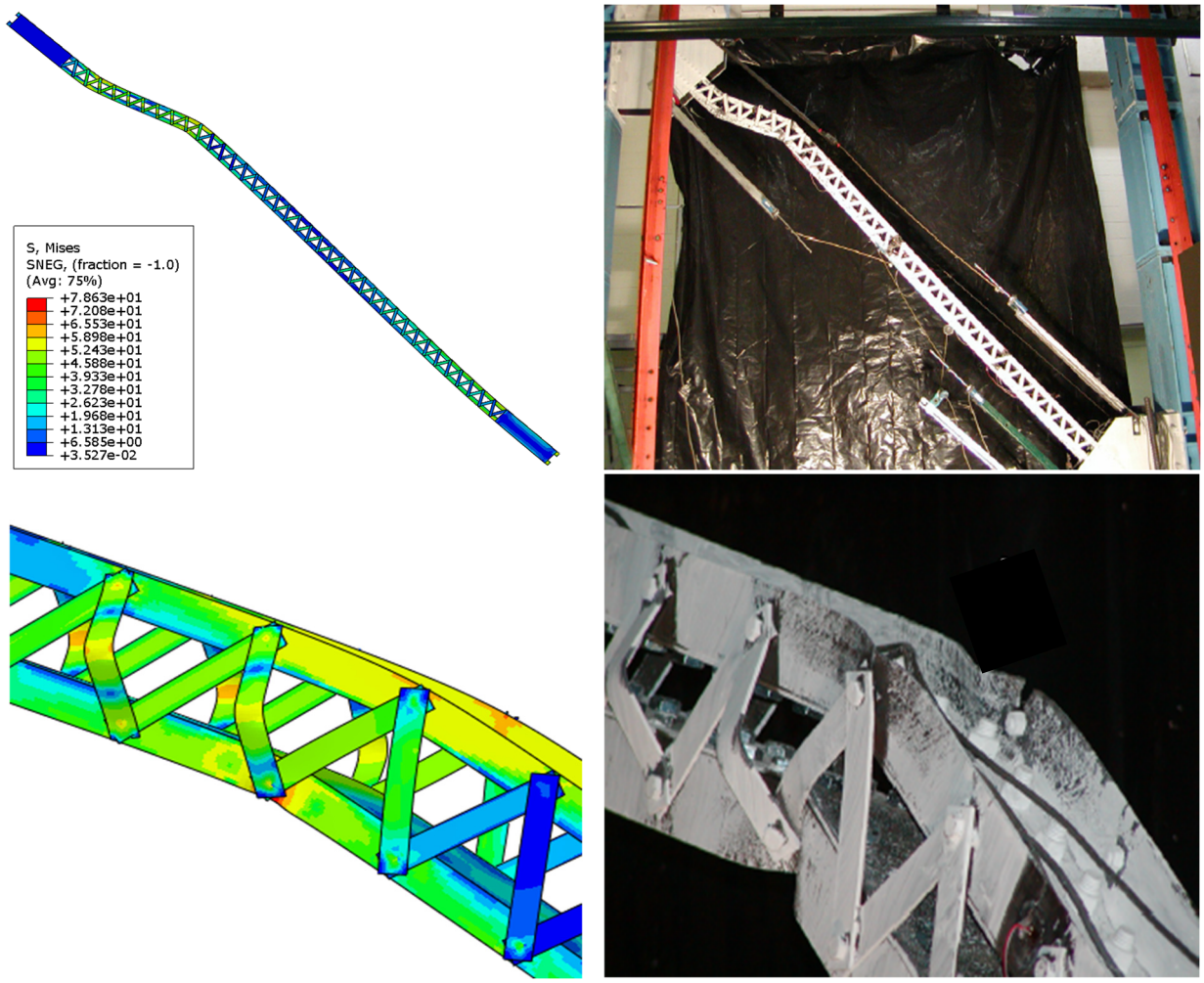

Figure 10: Comparison between test and FE failure modes for Specimen By8-120 reported in (Lee and Bruneau 2008) – (stress is in ksi).

As presented in Table 2, FE models subjected to cyclic loads show excellent agreement with experimental results, with an average $N_{u,FE}$ / $N_{u,test}$ ratio of 1.013 and a Coefficient of Variation (C.o.V.) of 5.9% for cyclic loading (Case 1). For static loading conditions (Case 2), the results also show improvement, with an average $N_{u,FE}$ / $N_{u,test}$ ratio of approximately 1.0, with a C.o.V. of 6.5%. Figure 9a shows that the hysteresis of specimen 3 obtained from FE model superimposed with the hysteresis of test results. There are no significant differences in the initial stiffness and maximum compression strength between FE and test results, showing that the impact of discontinuous yielding phenomenon has less impact for quad-linear stress-strain models at the initial yielding stage. The FE models accurately capture both the initial stiffness, ultimate resistance and post-peak response of the specimens, as depicted in the load-displacement curves for specimens in Group 2 and Group 4 (Figure 9b).Additionally, Figure 10 illustrates that the numerical failure mode of Specimen By8-120 aligns closely with the test result.

Strong correlation between FE predictions and test results are also observed for all specimens tested by Bonab et al. (Bonab et al. 2013) and Kalochairetis et al. (Kalochairetis et al. 2014), as shown in Table 3. The mean value of $N_{u,FE}$ / $N_{u,test}$ ratio is 0.985 with a C.o.V. of 6.3 %. Combined, all these results evidence that the developed numerical models reliably predict ultimate resistances and adequately capture the buckling behavior of laced built-up members, making them suitable for additional sub-studies and further numerical investigations.

Table 4: Comparison between test and FE results for various amplitudes of $e_{0,gloabl}$.

References	Specimens	Lacing system	Ultimate loads and ratios (Case 2)				
				Local amplify: $e_{0,local} = a_i$ / 200			
				Global amplify: $e_{0,global}$			
				L / 3000	L / 1500	L / 1000	L / 500
			N_{test} (kN)	$N_{u,FE}$ / $N_{u,test}$ (-)	$N_{u,FE}$ / $N_{u,test}$ (-)	$N_{u,FE}$ / $N_{u,test}$ (-)	$N_{u,FE}$ / $N_{u,test}$ (-)
(Astaneh-Asl et al. 1998; Kleiser and Uang 1999)	Specimen 1	Double	928.79	0.96	0.96	0.96	0.96
	Specimen 2		1633.83	1.01	1.01	1.00	0.98
	Specimen 3		2885.12	0.95	0.92	0.90	0.85
(Lee and Bruneau 2008)	By8-120	Single	295.81	1.19	1.13	1.07	0.95
	By16-60		521.64	1.12	1.07	1.02	0.91
	By16-120		447.00	1.25	1.17	1.11	0.98
	Bx8-60		267.16	1.26	1.21	1.16	1.05
	Bx8-120		213.51	1.36	1.29	1.24	1.11
	Bx16-60		506.87	1.30	1.29	1.29	1.09
	Bx16-120		409.50	1.28	1.20	1.15	1.02
(Kalochairetis et al. 2014)	Group 1	Double	200.00	1.08	1.08	1.07	1.06
	Group 2		206.00	1.06	1.06	1.05	1.04
	Group 4		230.00	1.08	1.07	1.07	1.07
	Group 5		247.00	1.04	1.02	1.03	1.01
			Mean	1.139	1.106	1.081	1.006
			C.o.V.	11.7 %	10.4 %	9.6 %	7.3 %
			Min.	0.954	0.925	0.903	0.845
			Max.	1.363	1.295	1.289	1.110

2.3 Influence of slenderness of lacing members

This section investigates the influence of the lacing members' slenderness on both the ultimate load and the shear force-to-ultimate load of built-up members. The studies cover various member lengths; therefore, a nondimensional unit is denoted as λ_{lacing} the slenderness of lacing members

and as λ_B for the slenderness of built-up members. For the lacing members, the expression for slenderness is given as:

$$\lambda_{lacing} = \sqrt{\frac{A_d f_y}{\pi^2 EI_d / d^2}} \tag{3}$$

where A_d is the total area of lacing bar, I_d is the minimum second moment of inertia, and d is the length of lacing bar.

Similarly, the relative slenderness of built-up members defined as:

$$\lambda_B = \sqrt{\frac{A_g f_y}{\pi^2 EI_g / L^2}} \tag{4}$$

where A_g is the total area of the section, I_g is the overall second moment of ineritia of the built-up member, and L is the length of the member.

A total of 168 numerical simulations of laced built-up columns with steel grade A36 (F_y = 250 MPa) were conducted, using both single and double lacing systems; also, the slenderness of lacing members (λ_{lacing}) were varied from 0.5 to 2.5. Each column was composed of two hot-rolled channel sections (C380x50.4). The relationship between the overall slenderness of built-up members (λ_B) and their ultimate resistance (N_u / Af_y) is presented in Figure 11. Figure 12 further illustrates how λ_B relates to shear force-to-ultimate load ($V_{u,2nd} / N_u$), as influenced by varying slenderness values of the lacing members. A detailed analysis of these results reveals that the slenderness of lacing members has a notable impact on the resistance to compression of built-up members with a single lacing system. For columns with λ_B ranging from 0.6 to 1.5, these members are more affected by global instability of lacing members, as characterized by their slenderness values.

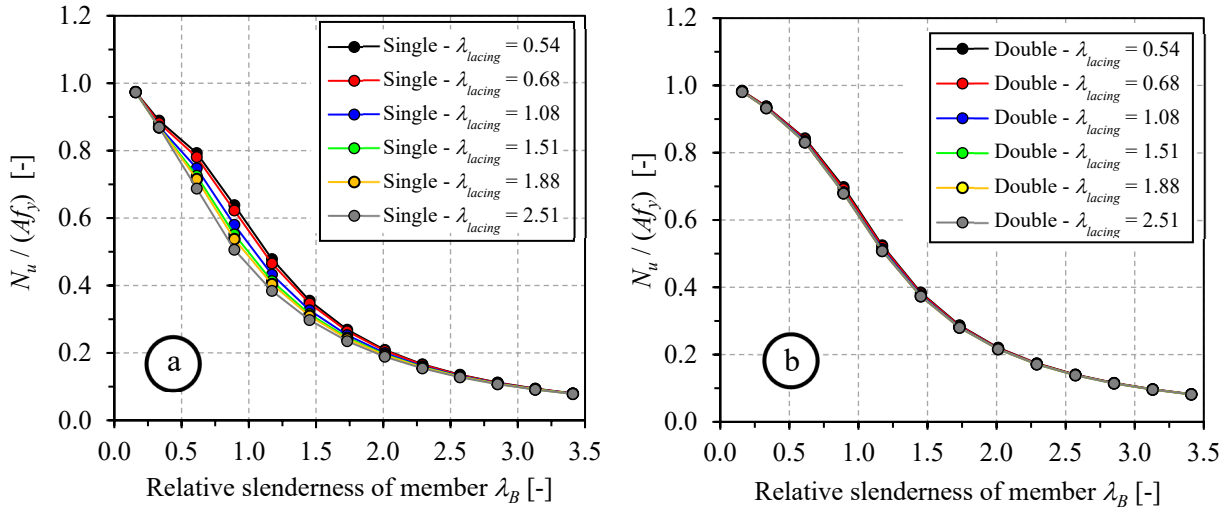

Figure 11: Influence of slenderness of lacings on ultimate load – (a) Single lacing system – (b) Double lacing system.

As depicted in Figure 11a, one reports an approximately 10% difference in carrying capacity for $\lambda_{lacing} = 0.54$ and $\lambda_{lacing} = 1.08$, and as much as a 20% difference between $\lambda_{lacing} = 0.54$ and $\lambda_{lacing} = 2.51$. In contrast, the global instability of lacing members with a double lacing system has a minimal impact on built-up members. It is important to remind that the shear forces within the lacing system are transferred along the axial direction of each lacing member. Lacing members in a single system primarily resists compression, which significantly affects global instability. However, lacing members in a double system resists both compression and tension, with one lacing member in compression and another in tension. This improves the performance of the compressed lacing member by balancing it through the tensioned lacing member.

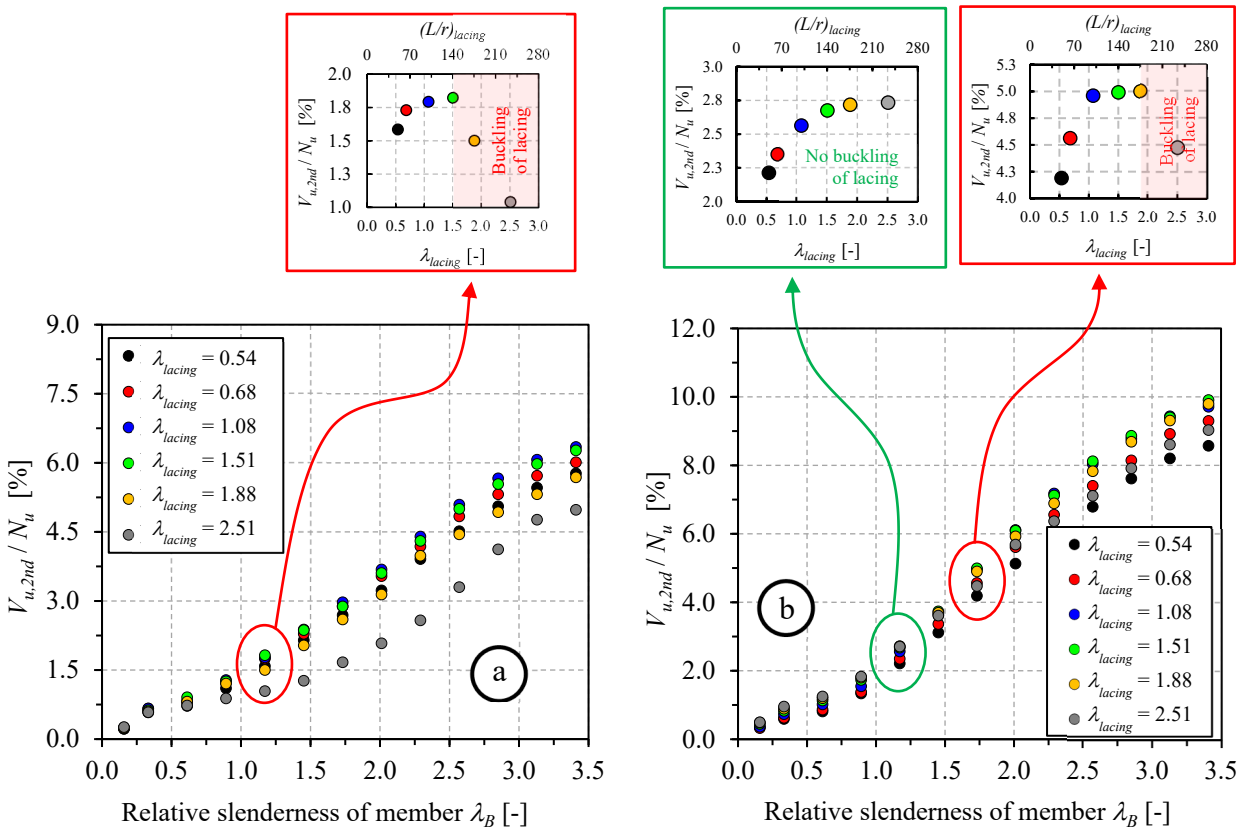

Figure 12: Influence of slenderness of lacings on shear force in built-up member – (a) Single lacing system – (b) Double lacing system.

Before the built-up member may reach its maximum carrying capacity, buckling in lacing members is observed in single lacing systems, especially when $\lambda_{lacing} > 1.5$. As illustrated in Figure 12a, for $\lambda_B \approx 1.25$, the percentage of $V_{u,2nd} / N_u$ relative to λ_{lacing} steadily increases before sharply decreasing when $\lambda_{lacing} > 1.5$ or $(L/r)_{lacing} > 140$ (see red ellipse) which the shear capacity of built-up members tends to be altered by early buckling in braces. For double lacing systems, particularly for built-up members with $\lambda_B < 1.5$, no buckling of lacing members is reported, demonstrating the advantage provided by the presence of two lacing bars. For an example, this is clearly observed for $\lambda_B \approx 1.25$ (see green ellipse in Figure 12b), where the percentage of $V_{u,2nd} / N_u$ consistently increases. However, similarly to the single lacing system, the first instance of buckling in double lacing members appears for $\lambda_B = 1.75$ when $\lambda_{lacing} = 1.88$ or $(L/r)_{lacing} = 175$ (see red ellipse in Figure 12b). This behavior arises due to the loss of redundancy of lacing members in double lacing,

especially for diagonals under tension. This loss of redundancy causes the compressed diagonal to begin buckling.

3. Proposed design equations

The previous sections conducted a series of sub-studies on chord arrangement, type of lacing system, and lacing slenderness for specific cross-sections. In this section, results of extensive parametric studies are reported using the validated numerical models to analyze how variations in section dimensions, section/member/lacing slenderness affect the overall resistance of laced built-up members. Approximately 1 600 computational models of laced built-up members were considered to determine the ultimate loads of columns and their corresponding shear force-to-ultimate load ratios (V_u / N_u). The numerical studies comprised the following parameters and criteria:

- The material properties of the lacing members and tie-plates were assumed to be similar to those of the main components of the built-up members, using steel grade A36 with a yield strength of $f_y = 250\ MPa$;
- The built-up columns consisted of two hot-rolled channels and C-shape sections arranged either tip-to-tip or back-to-back. The height-to-width (h / b) ratio of each channel and C-shape section was varied from 2.3 to 9. These hot-rolled sections include both non-slender and slender elements, with the web plate slenderness ratio h / t_w ranging from 6 to 65.8 and the flange plate slenderness b / t_f ranging from 4.9 to 20;
- Both main chords are widely spaced and connected by flat lacing bars arranged in X-configuration (double lacing), V-configuration or diagonal (single lacing) at intermediate spans, and by tie-plates at both ends. As discussed in the previous section, the slenderness of the lacing bars must be limited to prevent failure before the built-up members. Therefore, five relative slenderness ratios of the lacing bars (λ_{lacing}) were considered for each cross-section and varied from 0.5 to 1.88, associated with eight slenderness ratios of the built-up members (λ_B). Results have been used to propose equations to predict second-order shear force in laced built-up members in the following next sections.

3.1 Design proposal for double (X) lacing system

As previously mentioned, the investigation aims to provide a reliable, accurate and efficient design proposal for various ranges of built-up sections in compression, analyzing how variations in section dimensions and member/lacing slenderness affect the shear force in laced built-up members. The proposed equations are based on the assumption that the main components of built-up members are designed to reach their ultimate load before that of the lacing system. Therefore, the proposed equations are presented in the form V_u / N_u, where V_u is the shear force and N_u is the ultimate load, as a function of relative slenderness of built-up members, λ_B. For section dimensions of the main components, a key parameter is denoted as:

$$\gamma_V = \frac{\left(h / t_w\right)^2}{\left(b / t_f\right)} \tag{5}$$

γ_V which lies as an indication of the influence of the webs compare to flanges slenderness for the C-shape sections on the shear force acting along laced built-up sections. In Eq. 5, h is the height of the web of C-section, b is the width of the flange, and t_w and t_f are the thicknesses of web and

flange, respectively. A larger γ_V suggests that the web is significantly slenderer than the flange, i.e., web is much slenderer compared to flange. In such cases, the web responds more to section stability. In contrast, a lower value of γ_V indicates that web and flange have similar slenderness or that the flange governs the section response. As presented in Figure 13a, an increase in γ_V results in increasing ratio of V_u / N_u, meaning that shear force governs by the web slenderness. However, for built-up sections which the shear force is in a direction parallel to the flange of C-shape sections, the response to shear will primarily depends on the flange slenderness. Therefore, γ_V is expected to be lower. The proposed equations for the design shear force of members are summarized in Table 5, where γ_V characterizes how the plate slenderness of the main component of built-up members influences the shear force acting in built-up members. The parameters n, α_e and β are a curve fitting parameter, an equivalent factor that considers the influence of lacing slenderness – calibrated from numerical results – and a lacing arrangement factor, respectively.

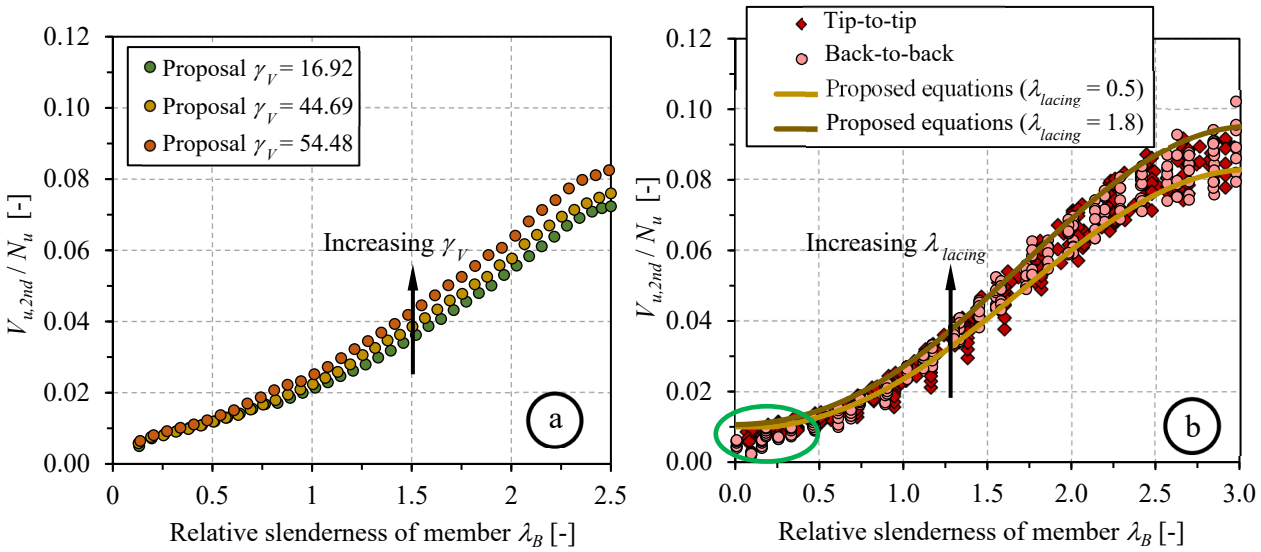

Figure 13: (a) Key parameter for section dimensions ( ) – (b) Proposal for laced built-up sections with double (X) lacing system.

The results of the parametric studies are presented in Figure 13b for tip-to-tip and back-to-back laced built-up sections with double (X) lacing systems. Figure 13b plots the recommended V_u / N_u curve for various range of the slenderness parameter of lacing members (λ_{lacing}) alongside all numerical results presented in the $V_u / N_u - \lambda_B$ format. From the observed trends, increasing λ_{lacing} values result in the curve shifting upward, indicating that built-up members with more slender lacing members exhibit a higher V_u / N_u value. As expected, the increase in V_u / N_u results from the slightly dropped ultimate carrying capacity of the built-up column due to the early buckling in lacing members. Note, however, that the slenderness of lacing members was limited to max. 1.8 to prevent the lacing systems from buckling before the built-up member does, as explained in Section 2.3. Additionally, for very short members with $\lambda_B \leq 0.25$, the ultimate load (N_u) has been observed to exceed the plastic resistance ($N_{pl} = A \cdot f_y$) due to strain hardening, resulting in a lower V_u / N_u ratio (see green ellipse). This effect is more pronounced in members with fewer than 3 modules (3 numbers of lacings). Thus, the minimum shear force-to-ultimate resistance ratio is constrained to 1% ($V_{u,\min} = 0.01 N_u$).

Table 5: Definition of parameters considered in the proposed equation for double (X) lacing system.

For $\lambda_B \le 0.25$	For $0.25 < \lambda_B < 2.5$		
$\frac{V_u}{N_u} = 0.01$	$\frac{V_u}{N_u} = \frac{\left[1.5 - \cos(\lambda_B)\right]^{1/n}}{\alpha_e \beta} \ge V_{u,\min}$		
	$\alpha_e = 41.8 - 3.4\lambda_{lacing} - 0.0017\gamma_V$		
	β	γ_V	n	λ_{lacing}
	1.0	$(h/t_w)^2 / (b/t_f)$	$0.7 + \lambda_B / 50$	≤ 1.8

3.2 Design proposal for single (diagonal) lacing system

To maintain continuity, the proposed equation for single lacing system is derived from the equation for the double lacing system. The results of the numerical studies are presented in Figure 14 for tip-to-tip and back-to-back laced built-up sections with single (diagonal) lacing systems. A comparison between Figure 13b and Figure 14a reveals that the shear force-to-ultimate load ratio (V_u / N_u) for built-up sections with double lacing system is greater than built-up sections with single lacing system. The difference shall be attributed to the greater shear stiffness of built-up members with a double lacing system. To further quantify this overall disparity, the shear force in the double lacing system is related to the shear force in the single lacing system, denoted as the $[V/N]_{u,double} / [V/N]_{u,single}$ ratio.

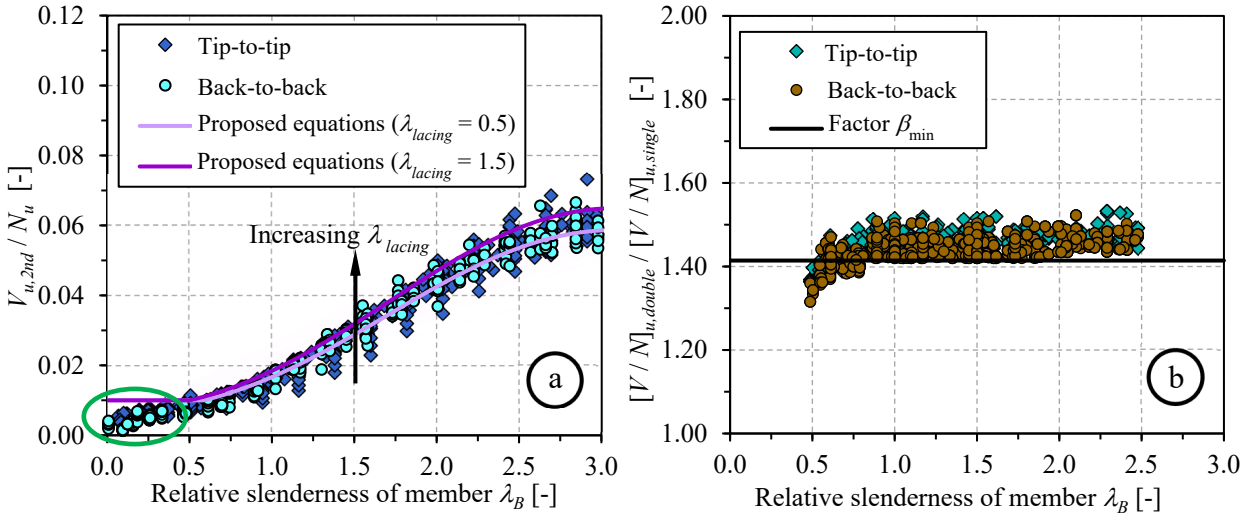

Figure 14: (a) Proposal for laced built-up sections with single lacing system – (b) Parameter for lacing arrangement (β).

Figure 13b illustrates this ratio as a function of λ_B for tip-to-tip and back-to-back built-up sections. Generally, the variation in shear force between double and single lacing systems range from 1.4 to 1.5 for built-up members with $\lambda_B > 0.75$; however, for members with $\lambda_B \approx 0.5$, the ratio scatters below 1.4 due to the presence of fewer than 3 modules in the built-up member. To ensure a conservative design approach, the minimum variation between shear force in double and single lacing systems is denoted as $\beta_{\min}$, approximately equal to 1.4 (see Figure 14b). This value is approximately equal to $\beta_{\min} \approx \sqrt{2}$ or can be expressed in terms of the variation in shear stiffness as $\beta_{\min} \approx \sqrt{S_{v,double} / S_{v,single}}$ where $S_{v,double}$ and $S_{v,single}$ represent the shear stiffness of the built-up

members with double and single lacing, respectively. Therefore, a design equation for members with single lacing systems can be adjusted by choosing β appropriately. The modified parameters used in the proposed equations for single (diagonal) lacing system are summarized in Table 6. Similar to members with a double lacing system, the minimum shear force-to-ultimate resistance is limit to 1%, particularly for members with $\lambda_B < 0.5$, and the slenderness of lacing members is restricted to $\lambda_{lacing} \leq 1.5$.

The first proposed equations for built-up members with both double and single lacing systems are summarized in Table 5 and Table 6, respectively. Note that the V_u / N_u function in both proposals relies on the same equation, making it an adaptive function capable of capturing the shear force level in different lacing configuration and various chord section dimensions. In the formulation, β accounts for variations in lacing arrangement, while γ_V take into account the influence of the section dimensions of the main components. Additionally, the equation is applicable to various slenderness levels of lacing members, enabling it to account for bending effects within the lacing system. However, the equations are moderately more intricate than those in the current practical rules due to the inclusion of the various parameters and the bending curvature factor (n). Consequently, a simplified format is proposed in the next section by combining uninfluential parameters into the bending curvature.

Table 6: Refined parameters considered in the proposed equation for single (diagonal) lacing system.

For $\lambda_B \leq 0.5$	For $0.5 < \lambda_B < 2.5$		
$\frac{V_u}{N_u} = 0.01$	$\frac{V_u}{N_u} = \frac{\left[1.5 - \cos\left(\lambda_B\right)\right]^n}{\alpha_e \beta} \geq V_{u,\min}$		
	$\alpha_e = 41.8 - 3.4\lambda_{lacing} - 0.0017\gamma_V$		
β	γ_V	n	λ_{lacing}
$\sqrt{2}$	$\left(h / t_w\right)^2 / \left(b / t_f\right)$	$1/\left(0.7 + \lambda_B / 50\right)$	≤ 1.5

3.3 Simplified design equations

In Section 3.1 and 3.2, equations for estimating the design shear force in laced built-up members were proposed. To facilitate manual calculations or integration into spreadsheet programs, simplified design equations have been developed; in this context, by elimination of γ_V and multiplication of the lacing arrangement factor β with a_e, equations for V_u / N_u in Table 5 and Table 6 reduce to:

$$\frac{V_u}{N_u} = \frac{\left[1.5 - \cos\left(\lambda_B\right)\right]^n}{\alpha} \geq 0.01 \tag{6}$$

Where $\alpha = 41.8 - 3.4\lambda_{lacing}$ for double (X) lacing system

$\alpha = 59 - 44.8\lambda_{lacing}$ for single (diagonal) lacing system

The only remaining parameter that shall further be modified is the factor n. Based on different standardized cross-section shapes catalogues such as the American, Canadian, European steel C-

shapes, γ_V was found to vary from 2.6 to 853.8. Yet, γ_V is more practically reported to range from 153.8 to 1080 in existing truss bridges. Associated n values range from $n = 1.36$ to 1.39. In this respect, the most appropriate choice of n is set as $n = 1.38$; this choice can be shown to minimize the difference between the first proposed equations in Section 3.1 and 3.2 and the simplified equation Eq. (6). The set of simplified equations for shear force in laced built-up members are presented in Table 7, which proposes two functions for calculating the factor α for different lacing arrangements.

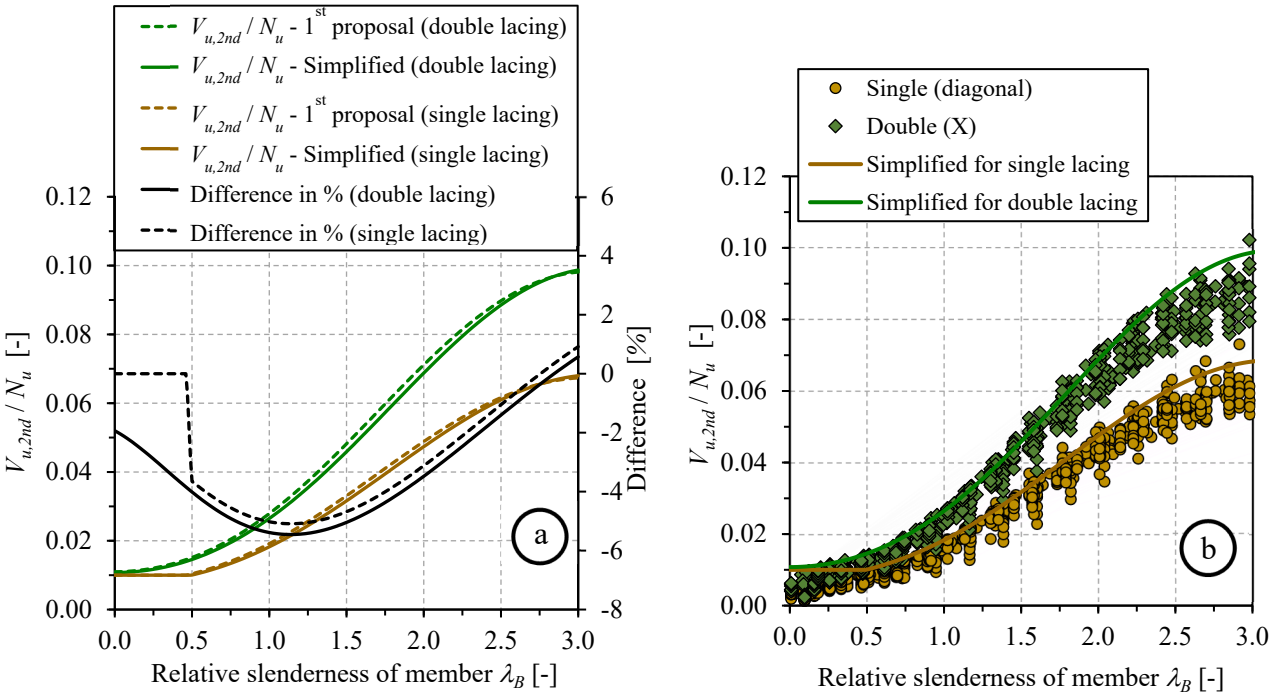

Figure 15: (a) Direct comparison and percent difference between the first proposed equation and the simplified equation with $n = 1.38$ – (b) Comparison of lacing arrangements with simplified equations.

Figure 15a shows a comparison between the first equation proposed in section 3.1 and 3.2 with the simplified equation with $n = 1.38$. To illustrate the maximum variation, the results in Figure 15a are plotted using $\gamma_V = 1080$, and $\lambda_{lacing} = 1.5$ and 1.8 for single and double lacing system, respectively. This represents the worst-case scenario, with all other cases exhibit better agreement. As indicated, the difference between these equations never diverged by more than approximately 5% for single lacing and 6% for double lacing. A negative value means that the simplified equation is less conservative than the first proposed equation, while a positive value shows that it is more conservative. Additionally, the comparison between lacing arrangements based on numerical results from the parametric studies is plotted in Figure 15b, along with their typical simplified curves for $\lambda_{lacing} = 1.5$ and $\lambda_{lacing} = 1.8$ for single and double lacing systems, respectively. The figure examines the behavior of single lacing systems and double lacing systems in terms of $V_{u,2nd} / N_u$ as a function of the slenderness parameter λ_B. It observed that single lacing systems exhibit a lower shear force-to-ultimate load ratio across all slenderness parameters. Oppositely, the double lacing system illustrates significantly greater values and a steeper increase with λ_B, indicating a stronger shear capacity. The typical simplified curve for a single lacing system is plotted for $\lambda_{lacing} = 1.5$, closely following the trend of finite element results of a single lacing

system, while the simplified curve for a double lacing system for λ_{lacing} = 1.8 also aligns well with the finite element results.

Table 7: Summary of simplified equations for shear force in laced built-up members.

$\frac{V_u}{N_u} = \frac{\left[1.5 - \cos\left(\lambda_B\right)\right]^n}{\alpha} \geq 0.01$
$\alpha = \begin{cases} 41.8 - 3.4\lambda_{lacing} & \text{for double lacing (X)} \\ 59 - 4.8\lambda_{lacing} & \text{for single lacing (diagonal)} \end{cases}$
$n = 1.38$
$\lambda_{lacing} \begin{cases} \leq 1.8 & \text{for double lacing (X)} \\ \leq 1.5 & \text{for single lacing (diagonal)} \end{cases}$

3.4 Performance of proposal and current design approaches against numerical results

The prediction of shear forces from the proposed equations is compared with three current design specifications: Eurocode (EC 3) and the American Standards (AASHTO) for laced built-up columns. Figure 16 (double lacing systems) and Figure 17 (single lacing systems) depict the performance of these current design approaches alongside the proposed equations for built-up columns with single (diagonal) and double (X) lacing systems. The ratio $V_{u,FE}$ / $V_{u,Ref.}$ represents the shear force predicted by the various design rules compared to the FE results obtained from the previously-described parametric studies. A ratio $V_{u,FE}$ / $V_{u,Ref.}$ greater than unity indicates that the design rules are on the unsafe side, whereas a ratio less than unity indicates that the design rules are on the safe side.

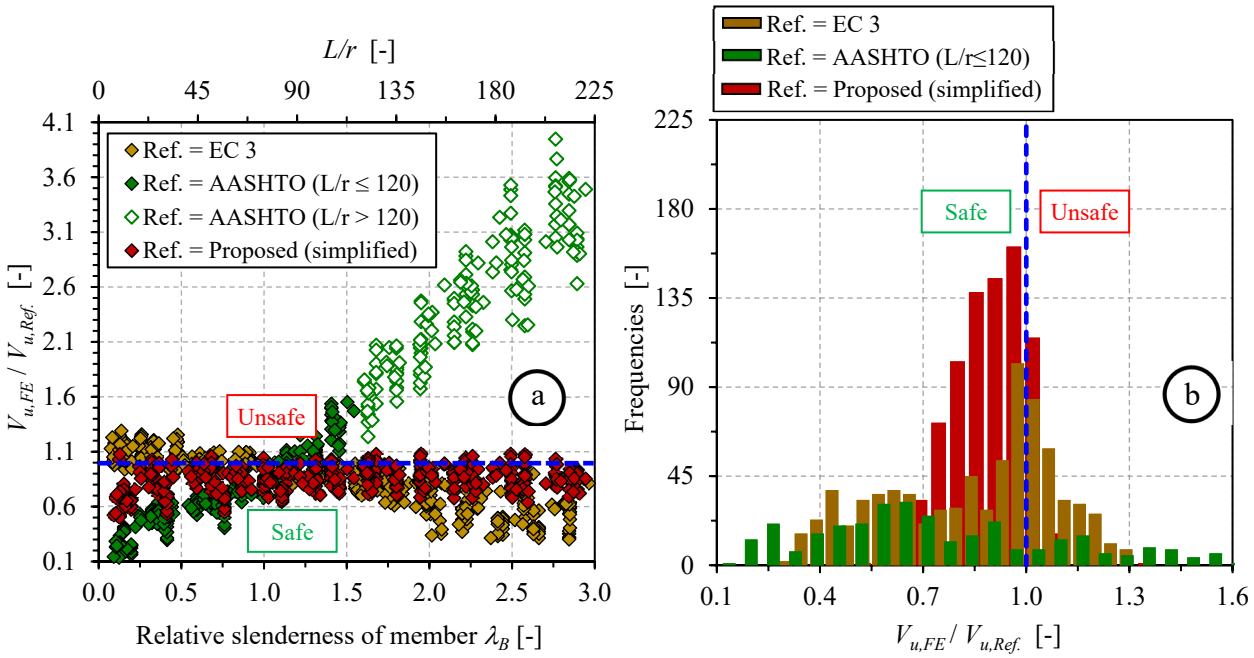

Figure 16: Design rules vs. numerical results for double lacing systems.

Figure 16a and Figure 17a illustrate the evolution of the $V_{u,FE}$ / $V_{u,Ref.}$ ratio with member slenderness (λ_B and L/r), while the associated frequencies are plotted in Figure 16b and Figure

17b. Additionally, the statistical data, including mean value, Coefficient of Variation (C.o.V.), maximum ratio, and minimum ratio, are reported in Table 8. The table also shows the percentage of overestimation on the unsafe side for values exceeding 5%, 10%, and 30%. For laced built-up members with double lacing systems, observations can be made from Figure 17 and Table 8. Overall, the results indicate that the proposed equations provide relatively accurate predictions compared to all three design codes, with a mean $V_{u,FE}$ / $V_{u,Proposal.}$ value of 0.90 and a C.o.V. of 0.12. The maximum discrepancy compared to the numerical results remains 8% on the unsafe side. Eurocode 3 provides less accurate results compared to the proposed equations, with a mean value of FE results to Eurocode 3 of 0.82 with the C.o.V. of 0.30. The results obtained from the standard are 8% more conservative than those of the proposed design equations. However, EC 3 exhibits quite worse results with respect to safety, reaching approximately 29% on the unsafe side, particularly for members with $\lambda_B < 0.75$.

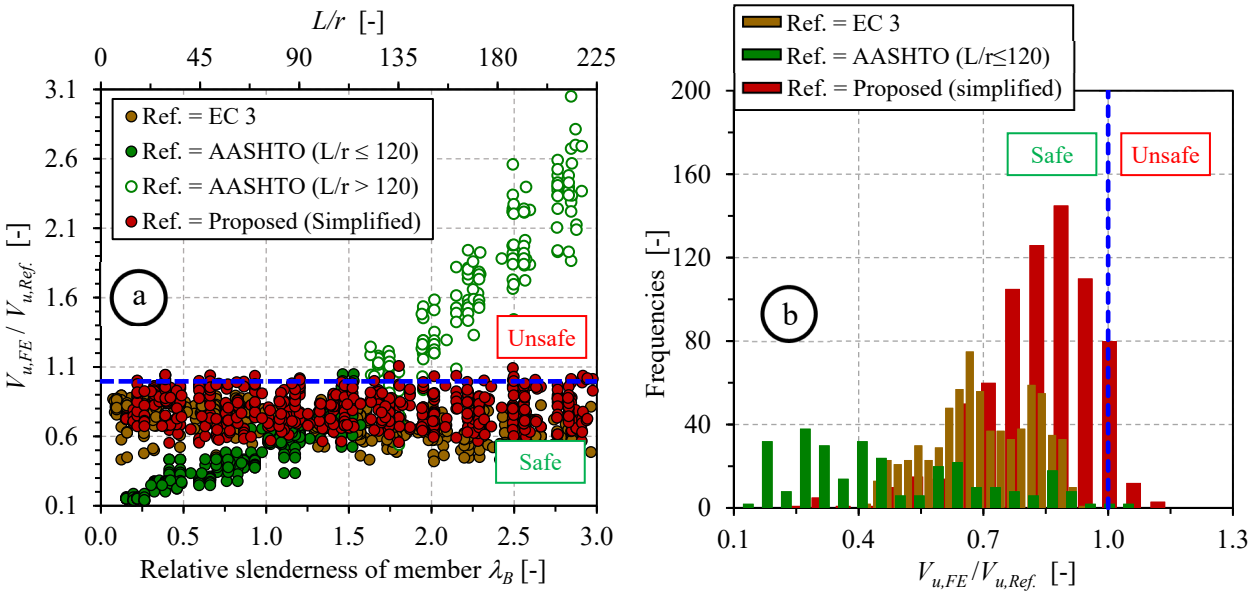

Figure 17: Design rules vs. numerical results for single lacing systems.

It is revealed that for members with $L/r \leq 120$, the results from AASHTO Provisions are overly conservative, with a mean value of $V_{u,FE}$ / $V_{u,AASHTO}$ ratio 0.72 and a C.o.V. of 0.48. A large value of C.o.V. indicates significant variability in results predicted by the AASHTO Provisions and needs to be refined of the provisions to improve the level of consistency, while the mean ratio of 0.72 reflects large scatter and lack of precision, particularly for members with $L/r < 30$ or $\lambda_B < 0.5$. Additionally, AASHTO Provisions also show unsafe predictions for members with L/r ranges between 90 and 120, with errors reaching up to 55% on the unconservative side, suggesting that its design recommendations might not be applicable for member slenderness within these ranges. Furthermore, the results turn out to be more severe for members with L/r ranges from 120 to 200 which the mean value of $V_{u,FE}$ / $V_{u,AASHTO}$ ratio reaches to 1.49 with a C.o.V. of 0.29 and 2.28 with a C.o.V. of 0.23 for built-up members with single and double lacing system, respectively (Table 8). The results indicate very unsatisfactory in terms of safety and cannot be reliable for members where the L/r value stands within this range. It could be observed that the shear force for laced built-up members, as suggested by the American Standards, is inconsistency. This reveals that potential improvement is required to enhance economic efficiency by exploring more flexible

options for various lacing arrangements, while also addressing safety concerns. Overall, the results for laced built-up members with double lacing systems demonstrate Eurocode 3 provides more accurate predictions than the American Standards, where most results are on the safe side. Additionally, the prediction obtained from Eurocode 3 turns out to be overly conservative for members where $\lambda_B > 1.75$, around 70% safer than the results obtained from FE models and being more than 20% more conservative than the proposed equation. However, the code also exhibits unsafe predictions for members where $\lambda_B < 0.5$; more than 25% are on the unsafe side, indicating that their equations are less applicable for all ranges of λ_B and lacing slenderness. In contrast, the proposed equation shows better accuracy, consistent across various lacing slenderness and member lengths.

Table 8: Statistical results of $V_{u,FE}$ / $V_{u,Ref}$ ratios for all members.

Lacing arrangements	References	Mean	C.o.V.	Max.	Min.	>1.05 (%)	>1.1 (%)	>1.3 (%)
Double lacings	EC 3	0.82	0.30	1.29	0.30	15.6	10.3	0.0
	AASHTO ($L/r \leq 120$)	0.72	0.48	1.55	0.14	7.9	6.9	3.4
	AASHTO ($L/r > 120$)	2.28	0.23	3.53	1.03	27.4	27.4	27.1
	Proposal (simplified)	0.90	0.12	1.08	0.51	2.4	0.0	0.0
Single lacings	EC 3	0.69	0.18	0.92	0.42	0.0	0.0	0.0
	AASHTO (L/r ≤ 120)	0.46	0.50	1.05	0.14	0.0	0.0	0.0
	AASHTO (L/r > 120)	1.49	0.29	2.56	0.54	23.3	22.5	15.7
	Proposal (simplified)	0.82	0.15	1.14	0.55	1.1	0.4	0.0

The results for built-up members with single lacing system are illustrated in Figure 17 and Table 8. In general, results of all design rules scatter on the safe side. The American Standards, specifically "AASHTO ($L/r \leq 120$)" gives the most conservative predictions with greatest dispersion, as evidenced by a mean value of 0.46 and a C.o.V. of 0.50. This significant variability highlights the need for enhancing the design rule, particularly for members with $L/r < 30$. The primary justification for this caution is that the American Standards assuming a constant ratio of shear force-to-ultimate load (i.e., $V_u / N_u = 2\%$) across all member lengths, particularly for L/r ratios less than 120, which leads to more conservative predictions for shorter members. It also observed that the shear force estimation derived from Eurocode 3 shows greater accuracy and less scattering compared to the American Standards, with approximately 20% better accuracy. A detailed analysis reveals that the main source of the observed differences lies in the shear stiffness factor (S_v), which is considered in Eurocode 3 for various lacing arrangements, whereas this parameter is overlooked in the design equations of the American and Australian standards. The proposed equations, on the other hand, achieve significantly higher accuracy and greater consistency. It is evident from Figure 16 and Figure 17 that the proposed equations for single lacing systems exhibit greater variation compared to those for double lacing systems. With a C.o.V. of 0.15 and a mean value of 0.82, which is more than 10% better than the present design rules, the suggested equations are still much more accurate than the other two design rules. Nevertheless, the mean value of $V_{u,\,FE}$ / $V_{u,Ref.}$ is still the best among the current design techniques. Therefore, the suggested equations can be viewed as an adequate equation in terms of consistency, precision, and safety due to the different member/lacing geometries, lacing configurations taken into consideration, and the potential buckling within of lacing members. Considering the diverse section dimensions, varying slenderness of lacing members, and different chord arrangements, the proposed equations for

predicting the acting shear force in laced built-up members, whether with double (X) or single (diagonal) lacings, prove to be an excellent alternative. They provide more accurate, consistent, and straightforward estimates compared to current design practices.

4. Conclusions

This paper investigated the buckling behavior of lacing systems in laced built-up members composed of two C-shapes under pure axial compression. To determine the second-order shear forces acting on laced built-up members resulting from imperfect members under compression, various parameters were examined using validated finite element models. Such the FE models were validated against 23 test data sets which the members comprised of various chords and lacing configurations, obtained from different laboratories. These parameters included different lacing arrangements, slenderness of lacing members, chord arrangements, geometric imperfections, and member lengths. Based on extensive FE numerical results, new equations were proposed for the shear force-to-ultimate load ratio (V_u / N_u) associated with member length to predict the second-order shear force acting in laced built-up members. The equations are applicable to range slenderness levels of lacing members, allowing them to account for instability effect of diagonal in the lacing system. These equations were then slightly simplified into a more practical format, making them useful for design practice. The performance of the proposed equations was compared with two existing design standards and assessed against the reference numerical results. It was found that Eurocode 3 tends to provide inconsistent and conservative predictions, while the American Standards is often excessively conservative and sometimes unduly scattered on the unsafe side, particularly for built-up members with double lacing systems when $L/r > 90$. In comparison, the proposed equations provide greater adaptability for various lacing configuration, better accuracy, higher consistency, and enhanced simplicity compared to existing design rules.

References

AISC. 2016. *Specification for Structural Steel Buildings*. ANSI/AISC 360-16, American Institute of Steel Construction, Chicago, IL.

American Association of State Highway and Transportation Officials, ed. 2020. *LRFD Bridge Design Specifications*. 9th edition. Washington, DC: American Association of State Highway and Transportation Officials.

AS 4100:2020. n.d. *Steel Structures, Standards Australia*. Sydney.

Astaneh-Asl, Abolhassan, Robert A. Dameron, Ahmad Itani, Alex Krimotat, and Chia-Ming Uang. 1998. "Proof-Testing of Latticed Members and Their Connections on SFOBB."

ATC. 1992. *Guidelines for Cyclic Seismic Testing of Components of Steel Structures*. No. ATC-24. Redwood City, Calif.

Beyer, André, Nicolas Boissonnade, Abdelouahab Khelil, and Alain Bureau. 2018. "Influence of Assumed Geometric and Material Imperfections on the Numerically Determined Ultimate Resistance of Hot-Rolled U-Shaped Steel Members." *Journal of Constructional Steel Research* 147:103–15.

Bonab, A. Poursamad, B. Hosseini Hashemi, and Mahmood Hosseini. 2013. "Experimental Evaluation of the Elastic Buckling and Compressive Capacity of Laced Columns." *Journal of Constructional Steel Research* 86:66–73.

Dassault Systèmes. 2022. *Abaqus/CAE*. Version 2022.

Duan, L., M. Reno, and Chia-Ming Uang. 2002. "Effect of Compound Buckling on Compression Strength of Built-up Members." *Engineering Journal* 39:30–37.

Gérard, Lucile, Liya Li, Markus Kettler, and Nicolas Boissonnade. 2019. “Recommendations on the Geometrical Imperfections Definition for the Resistance of I-Sections.” *Journal of Constructional Steel Research* 162:105716.

Gérard, Lucile, Liya Li, Markus Kettler, and Nicolas Boissonnade. 2021. “Steel I-Sections Resistance under Compression or Bending by the Overall Interaction Concept.” *Journal of Constructional Steel Research* 182:106644.

Iskander, G., E. Soliman, and E. Sayed-Ahmed. 2021. “Design of Built-up Steel Beam-Columns Composed of Two-Channel Sections.” *Canadian Journal of Civil Engineering* 48(11):1508–22.

Kalochairetis, Konstantinos E., Charis J. Gantes, and Xenofon A. Lignos. 2014. “Experimental and Numerical Investigation of Eccentrically Loaded Laced Built-up Steel Columns.” *Journal of Constructional Steel Research* 101:66–81.

Kleiser, Michael, and Chia-Ming Uang. 1999. “Steel Latticed Members under Cyclic Axial and Flexural Actions.” *Journal of Structural Engineering* 125(4):393–400.

Lee, Kangmin, and Michel Bruneau. 2008. “Seismic Vulnerability Evaluation of Axially Loaded Steel Built-up Laced Members I: Experimental Results.” *Earthquake Engineering and Engineering Vibration* 7(2):113–24.

Li, Liya, and Nicolas Boissonnade. 2022. “Local/Global Coupled Instabilities of Slender I-Sections under Compression.” *Thin-Walled Structures* 172:108842.

Li, Liya, Mario Fafard, and Nicolas Boissonnade. 2022. “Local and Global Instabilities of Rolled T-Section Columns under Axial Compression.” *Thin-Walled Structures* 178:109517.

Lindner, Joachim, and Torsten Glitsch. 2004. “Vereinfachter Nachweis für I- und U-Träger – beansprucht durch doppelte Biegung und Torsion.” *Stahlbau* 73(9):704–15.

prEN 1993-1-1:2020. 2019. *Eurocode 3: Design of Steel Structures – Part 1-1: General Rules and Rules for Buildings*. Doc. CEN-TC250-SC3_N3023.

Southwell, Richard Vynne. 1997. “On the Analysis of Experimental Observations in Problems of Elastic Stability.” *Proceedings of the Royal Society of London. Series A, Containing Papers of a Mathematical and Physical Character* 135(828):601–16.